J Mater Sci (2011) 46:938–950
DOI 10.1007/s10853-010-4838-0

Analyses of deformation twinning in the extruded magnesium alloy AZ31 after compressive and cyclic loading

Michael Huppmann · Martin Lentz · Sarkis Chedid · Walter Reimers

Received: 6 July 2010 / Accepted: 14 August 2010 / Published online: 28 August 2010

Abstract The influence of different loading conditions on the microstructural development of extruded magnesium alloy AZ31 was investigated by optical microscopy and electron backscattered diffraction. Extruded magnesium profiles exhibit a significant asymmetry in the mechanical properties, due to the low activation energy of the extension twinning system $\{10\bar{1}2\}\langle 10\bar{1}1\rangle$, when compressing along the extrusion direction. For the analyses of this twinning system, compression tests with different applied strains $0.4 \leq \varepsilon \leq 11\%$ were performed for two extrusion products exhibiting different microstructures. The main deformation mechanisms during cyclic loading are the formation of extension twins during compression and the detwinning during subsequent tensile loading. The strain-controlled fatigue tests were carried out with applied strain amplitudes $0.3 \leq \varepsilon_A \leq 5\%$. The tests were stopped at characteristic numbers of cycles N in the tensile or compression maximum of the hysteresis loop. The microstructural investigations deliver information about the type of twinning and the size, shape, local distribution, and volume fraction of twins as a function of the plastic deformation. These results will be discussed with regard to the microstructure of the initial state material and to the applied load.

Introduction

The understanding of the microstructural development during compression and cyclic loading is crucial for the application of magnesium alloys as structural material. Intensive work has been carried out in the last decade to achieve a better understanding of the properties and the deformation mechanisms of the magnesium alloy AZ31 [1–10].

It is common that extruded or rolled magnesium profiles exhibit a significant asymmetry in the quasi-static mechanical properties under tension and compression. The asymmetry of the quasi-static mechanical properties is caused by the $\langle 10\bar{1}0\rangle\langle 11\bar{2}0\rangle$ double fiber texture parallel to the extrusion direction and the low activation energy for the $\{10\bar{1}2\}\langle 10\bar{1}1\rangle$ twinning system (extension twins), when compressing along the extrusion or rolling direction [3, 5, 9–11]. The evolution of $\{10\bar{1}2\}\langle 10\bar{1}1\rangle$ extension twins as a function of the applied compressive load was studied by optical microscopy [9, 12], by acoustic emission [13] and by electron backscattered diffraction (EBSD) [12, 14]. Additionally in situ diffraction studies have been performed using neutrons [3, 5]. The in situ diffraction studies also gave evidence for the activation of $\{10\bar{1}1\}\langle 10\bar{1}2\rangle$ contraction twinning system after saturation of the extension twinning system at about $\varepsilon = 8\%$.

In the recent years especially the fatigue behavior of magnesium alloys has attracted interest. The first extended fatigue investigations were reported by Noster [15, 16], followed by studies of Hasegawa et al. [17] and others [18–22]. These authors focused on the macroscopic fatigue behavior and pointed out that the asymmetric, sigmoidal shaped stress–strain hysteresis loop is due to twinning and detwinning mechanism during cyclic loading [19, 20].

Also microstructural investigations on the formation of $\{10\bar{1}2\}\langle 10\bar{1}1\rangle$ extension twins at compression half cycle and the detwinning after load reversal and subsequent tensile loading were investigated by optical microscopy

M. Huppmann (✉) · M. Lentz · S. Chedid · W. Reimers
Department Material Science and Technologies, Chair Metallic Materials, Technische Universität Berlin, Berlin, Germany
e-mail: michael.huppmann@tu-berlin.de

[9, 23] and EBSD [24–26]. The studies figured out that most of the twins formed during compression disappear after subsequent tensile loading and smaller needle-shaped twins were formed.

In this study, the microstructure development during compression and strain-controlled low cycle fatigue tests was investigated by optical microscopy and EBSD for two different extrusion products with different microstructures.

Compression tests were carried out and stopped at defined applied strains ε to describe the microstructural changes as a function of the applied load. Especially the size, shape, local distribution, and volume fraction V_t of $\{10\bar{1}2\}\langle 10\bar{1}1\rangle$ extension twins were determined as a function of the applied strain ε. The characteristics of the extension twins were compared within the compression tests as well as with the results of cyclic loading tests. In order to analyze the grain size dependency of twinning and detwinning, differently extruded profiles, showing different grain size distributions, were compared.

The twinning–detwinning process was analyzed at characteristic number of cycles N at maximum compressive and tensile deformation to examine the influence of these deformation mechanisms on the cyclic failure. Therefore, the strain amplitude was varied in between $0.3 \leq \varepsilon_A \leq 5\%$ and the influence of ε_A on the characteristics of the twins will be discussed.

Material and experimental procedure

Material

The tested magnesium alloy AZ31 was processed by indirect extrusion at billet temperatures $T_B = 250$ and 270 °C. A press ratio $R = 25$ and a ram speed $v_{Ram} = 0.5$ mm/s were chosen. The chemical composition of the magnesium alloy AZ31 is shown in Table 1. The extrusion tests were carried out on the 8.32 MN rod and tube extrusion press of the Extrusion Research and Development Centre (ERDC) at the Technische Universität Berlin.

Table 1 Chemical composition of the magnesium alloy AZ31 (wt%)

Mg	Al	Zn	Mn	Si	Fe	Pb	Others
Balance	2.873	0.872	0.326	0.026	0.003	0.003	<0.003

The micrographs, taken from the longitudinal section (parallel to the extrusion direction), show some elongated grains for all extrusion products which remain from the former cast structure of the billets (Fig. 1). The microstructure in between those elongated grains differs due to the different billet temperatures. A billet temperature of $T_B = 250$ °C (Fig. 1a) results in very fine grain structure which occur due to dynamic recrystallization (DRX) and only a few DRX grains show static recrystallization (SRX) and grow up to a grain size of about $d \approx 20$–30 μm. In the following these samples are called series A.

At a billet temperature of $T_B = 270$ °C only a few DRX grains, with a very small grain size, were observed, while most of the former DRX grains coarsen to $d \approx 20$–50 μm due to the extended SRX behavior [10]. In the following these samples are called series B. Both the sample series exhibit a small amount of Al–Mn particles (black dots) with sizes up to a few microns. A more detailed analysis of the sample series A and B, concerning microstructure, texture, and mechanical properties are published in [10].

Experimental procedures

All mechanical tests were conducted with the servo-hydraulic testing machine MTS 810 at room temperature. The compression tests were performed with a strain rate of 2.5×10^{-4} s^{-1} and were stopped at defined applied strains $0.4 \leq \varepsilon \leq 11\%$, to analyze the microstructure, especially the amount and the characteristics of the $\{10\bar{1}2\}\langle 10\bar{1}1\rangle$ extension twins.

The typical compression stress–strain curve for the analyzed samples and the measurement points (gray

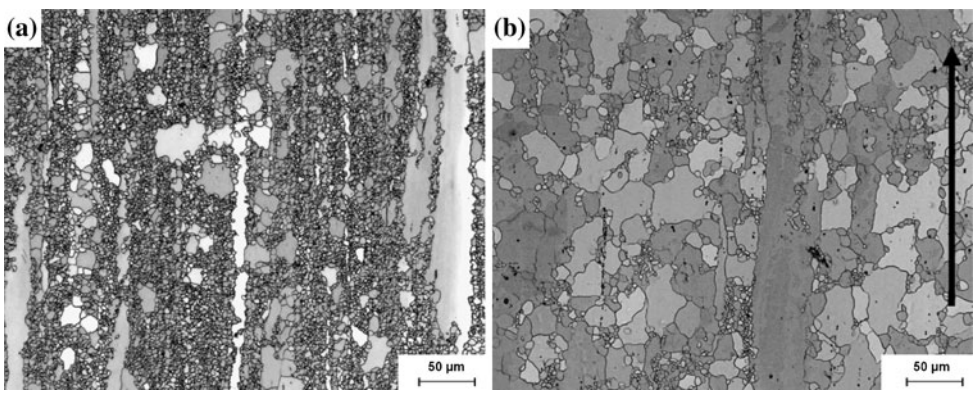

Fig. 1 Initial microstructure of the extrusion products (↑ extrusion direction): **a** series A and **b** series B

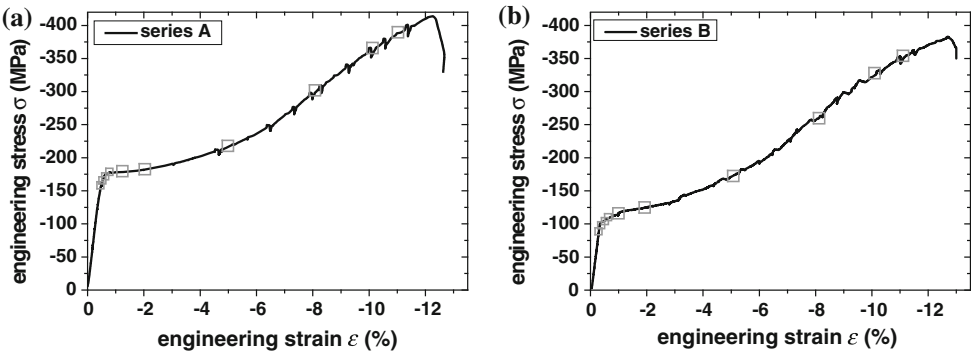

Fig. 2 Compression stress–strain curves for: **a** series A and **b** series B

squares) are shown in Fig. 2. The compression yield strength (CYS) of series A is about 50% higher than for series B. The ultimate compression strength (UCS) is only slightly higher for series A, while the fracture strain is slightly lower. Details of all mechanical properties are reported in [10].

The total strain controlled fatigue test were carried out at room temperature with a strain ratio $S = \varepsilon_{min}/\varepsilon_{max} = -1$. A sinus-shaped testing curve was applied with a frequency $f = 1$ Hz. The strain amplitude ε_A was varied between 0.3 and 5%. The tests were stopped at characteristic numbers of cycles N in the tensile or compression maximum of the hysteresis loop.

For the investigations by means of optical microscopy samples were prepared using a standard metallographic preparation [10] and given additional polishing step using 0.2 μm silica (Struers OPS). Finally, the samples were electropolished. Afterward the specimens were etched with picric acid solution containing 5-g picric acid, 6-mL acetic acid, 20-mL H_2O, and 100-mL ethanol.

The samples for the EBSD measurements were prepared in the same way without etching. The EBSD orientation maps with step sizes of 0.3 and 0.5 μm were obtained using a Hitachi S-2700 scanning electron microscope combined with a HKL-Nordlys-II detector. The EBSD measurements were conducted at the Zentraleinrichtung Elektronenmikroskopie (ZELMI) at the Technische Universität Berlin.

For the calculation of the volume fraction of twins V_t a simple point counting technique (ASTM E562-02) was used as it was suggested by [12]. Therefore, two micrographs with magnifications of 200 were analyzed for each compression sample. Using the image analysis software *ImageJ 1.42q* [27] a 162 point by 129 point grid was put on the samples which exhibit few fine and narrow twins ($\varepsilon \leq -0.625\%$) and a 87 point by 69 point grid was used for the samples with broader twins ($\varepsilon \geq -0.75\%$). The number of points which are within the twins divided by the total number of points result in the volume fraction of twins V_t. Additional analyses with the tool *Analyze Particles* of *ImageJ* were performed by defining a gray value threshold for the twins.

Results

Compression tests

The microstructural development for series A (Fig. 3) and series B (Fig. 4) as a function of the compressive strain ε is presented for the cross-sections of the compression samples. The plastic deformation under compression is delivered to a small amount by the activation of slip systems. However, the main contribution to the plastic deformation is due to the activation of the extension twinning system $\{10\bar{1}2\}\langle 10\bar{1}1\rangle$, the total amount of twins increases with increasing compressive strain ε for both initial microstructures. At first the development of extension twins for series A will be described. At $\varepsilon = -0.4\%$ (Fig. 3a) no twinned microstructure could be observed because plastic deformation is not present at this ε due to the relatively high CYS of series A. The first twins appear when the applied strain is slightly higher than the limit of elastic deformation ($\varepsilon = -0.5\%$ not shown here). According to the Hall–Petch relation the twinning starts in large grains, i.e., the elongated grains from the former cast structure, but the total volume fraction of twins is very small $V_t \approx 0.6\%$.

The twin formation starts only in these large grains resulting in an inhomogeneous distribution of twins. The twins have a needle-like shape, which converges at the grain boundaries. No twinned microstructure could be observed in the small grains ($d < 10$ μm). If the compressive strain is increased up to $\varepsilon = -0.75\%$ (Fig. 3b), the number and the V_t increase in large grains, while the broadening of the twins remains nearly constant. Consequently, the increase up to $V_t \approx 3.5\%$ is realized by the formation of new twins. Further compressive straining to $\varepsilon = -2\%$ (Fig. 3c) results in the formation of twins in smaller grains ($d = 5$–10 μm), which have a favored orientation for twinning. Also the existing twins in the large grains begin to broaden resulting in $V_t \approx 15\%$. At $\varepsilon = -2\%$ the shape of the twins is still regularly. At $\varepsilon = -5\%$ (Fig. 3d) volume fraction of twins increases very strong to $V_t \approx 40\%$, but in contrast to the first regime only a few

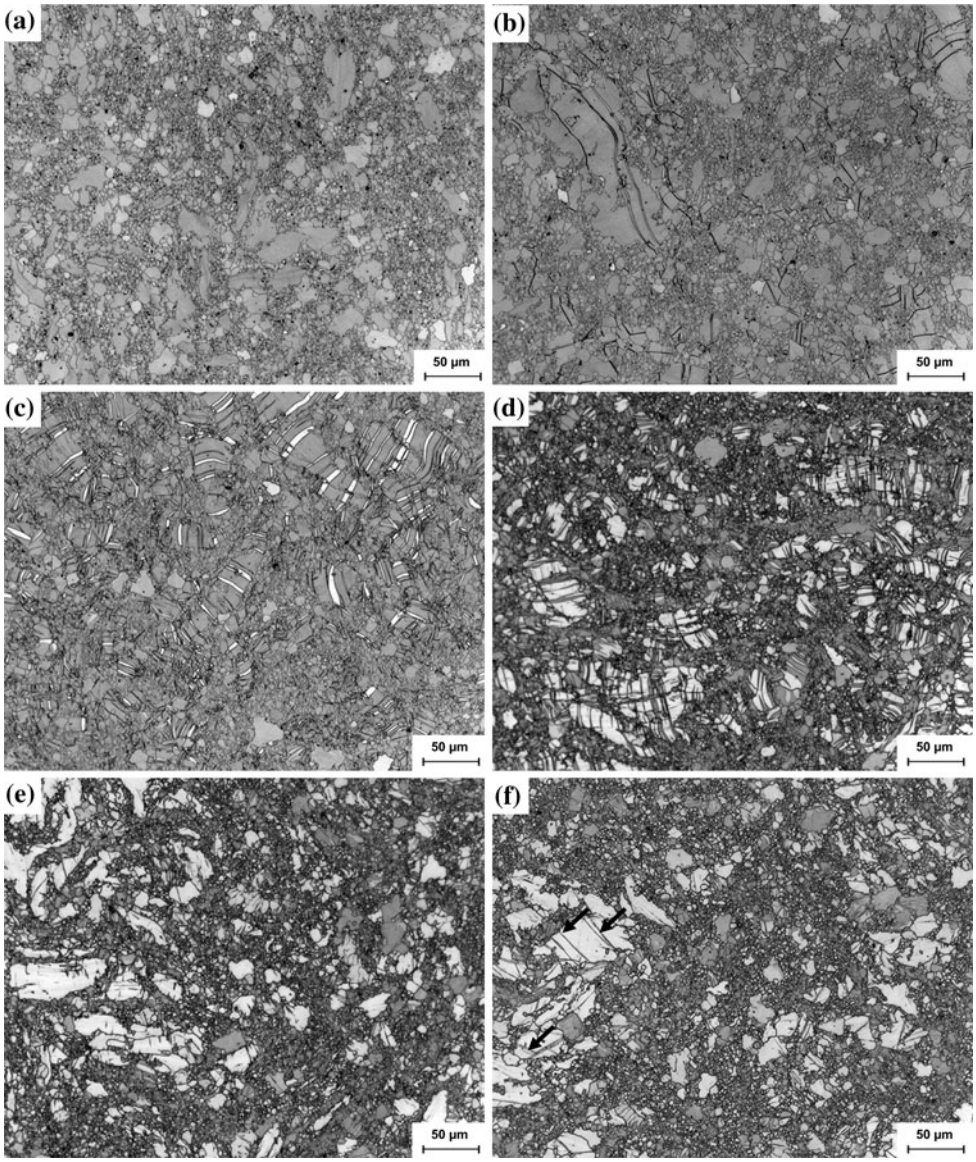

Fig. 3 Microstructural development (cross-sections) during compression (series A): **a** $\varepsilon = -0.4\%$, **b** $\varepsilon = -0.75\%$, **c** $\varepsilon = -2\%$, **d** $\varepsilon = -5\%$, **e** $\varepsilon = -8\%$, and **f** $\varepsilon = -11\%$

new twins were formed, but the existing twins are expanding. In the last regime at $\varepsilon = -8\%$ (Fig. 3e) the extension twinning mechanism is almost saturated and almost all grains larger than $d > 3$ µm show a completely twinned grain structure (white grains). Only a few lines inside the large grains indicate that some areas were not completely twinned. Some of the gray grains (Fig. 3e) with $d = 10$–20 µm are not twinned, because their orientation does not allow deformation twinning. Also the very small grains ($d < 3$ µm) did not undergo twinning, because the critical resolved shear stress (CRSS) for twinning is still not achieved. Before rupture at $\varepsilon = -11\%$ (Fig. 3f) again twin structures in the bigger grains were observed (black arrows). But the shape of these twin structures is thin and straight. Due to the fact that these large grains were reoriented by 86° due to the former compression deformation, their *c*-axis is now parallel to the loading direction. Thus, the activation the $\{10\bar{1}1\}\langle 10\bar{1}2\rangle$ contraction twinning system is favored [5] resulting in these new twin bands.

The microstructural development of series B (Fig. 4) during compression shows qualitatively the same behavior as shown for series A, but some differences due to the larger grain sizes are obvious. First of all twinning starts at lower compressive strains, because the CYS is lowered when compared to series A, thus the limit of elastic deformation is reached at $\varepsilon \approx -0.4\%$ and twinning takes place (Fig. 4a). Again twinning starts in the large grains and the twins have a needle-like shape, which converges at the grain boundaries. The twin formation starts mainly at agglomerates of larger grains with a few small grains in between, resulting in an inhomogeneous distribution of

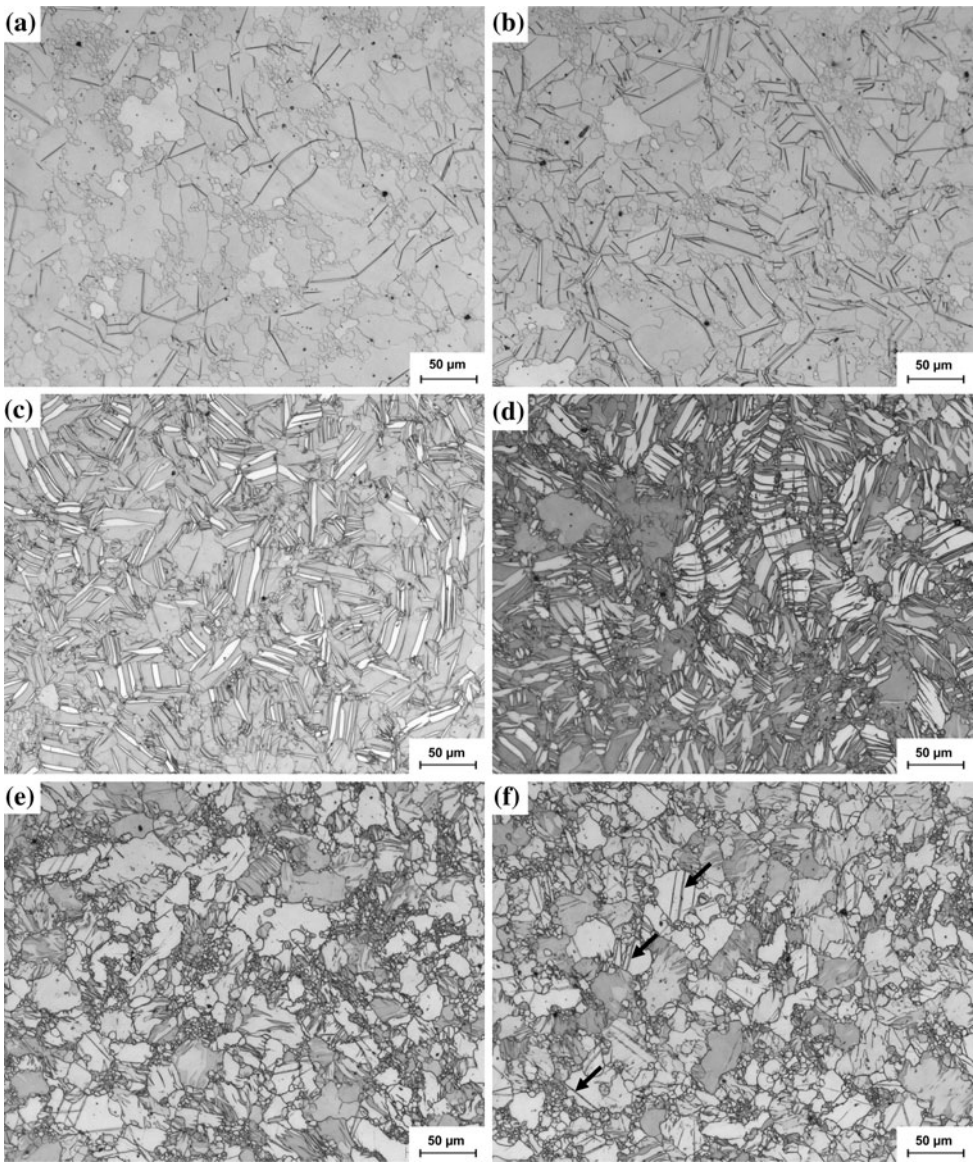

Fig. 4 Microstructural development (cross-sections) during compression (series B): **a** $\varepsilon = -0.4\%$, **b** $\varepsilon = -0.75\%$, **c** $\varepsilon = -2\%$, **d** $\varepsilon = -5\%$, **e** $\varepsilon = -8\%$, and **f** $\varepsilon = -11\%$

twin clusters. This isle-like formation is assumed to be caused by a stress concentration at the grain boundaries between these large and small grains.

At $\varepsilon = -0.4\%$ the $V_t \approx 3.1\%$ for series B and is almost as high as at $\varepsilon \leq -0.75\%$ for series A. If the compressive strain is increased to $\varepsilon = -0.75\%$ (Fig. 4b) the number of twins increases in large grains. The increase of $V_t \approx 12\%$ is mainly realized by the formation of new twins resulting in a more homogeneously distributed twin structure over the whole cross-section. Further compressive straining $\varepsilon = -2\%$ (Fig. 4c) and $\varepsilon = -5\%$ (Fig. 4d) again results in a higher number of twins, but in contrast to the first regime the existing twins are expanding. At $\varepsilon = -2\%$ the shape of the twins is still needle-like and regularly and $V_t \approx 20\%$. When the applied strain reaches $\varepsilon = -5\%$, the size of the twins is coarse and their shape is chunky and half of the microstructure has accomplished twinning. Only some of the very small grains and some of the larger grains, which are unfavorable orientated for twinning, exhibit no twin structures. In the last regime almost the entire microstructure consists of completely twinned grains and the twinning mechanism is almost exhausted at $\varepsilon = -8\%$ (Fig. 4e). Only a few lines inside the grains indicate that some areas were not completely twinned. Also the very small grains did not undergo twinning, because the CRSS for twinning is still not achieved. Before rupture at $\varepsilon = -11\%$ (Fig. 4f) again needle-shaped twin structures (indicated by black arrows) in the bigger grains were observed, which are caused by the $\{10\bar{1}1\}\langle 10\bar{1}2\rangle$ contraction twinning system.

The detailed analysis of the volume fraction of twins V_t as a function of the applied compressive strain ε is

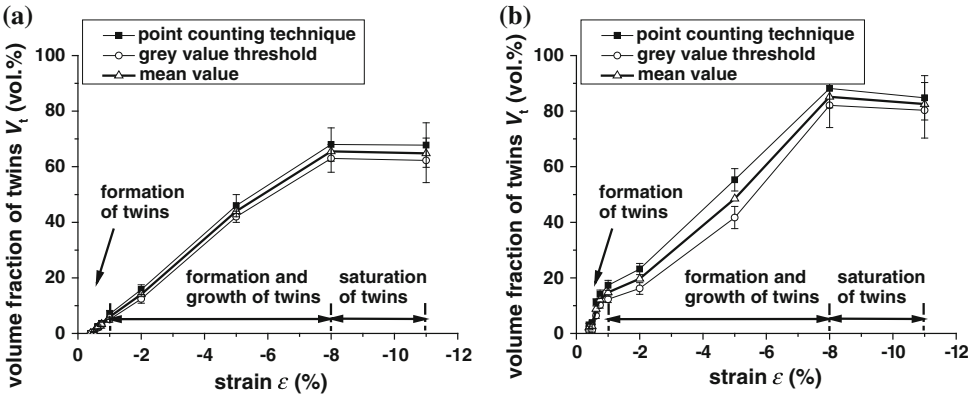

Fig. 5 Volume fraction of extension twins as a function of the applied compressive strain ε: **a** series A and **b** series B

presented for both the series (Fig. 5). The results are shown for the point counting technique and the gray value threshold (*Analyze Particles*) technique integrated in *ImageJ* [27]. The volume fraction of twins V_t obtained from both analyzing techniques differs slightly. The pointing count technique may overestimate the total volume fraction of twins, because points, which are not completely (but more than 50%) inside the twinned structure, were also assumed to be twinned area. The gray value threshold technique (*Analyze Particles*) technique underestimates V_t, because the chosen gray value thresholds were very strict to avoid the determination of artifacts, like precipitates and conventional grain boundaries resulting in an insufficient V_t. Averaging both results will give the most reasonable values for V_t.

Both the series show qualitatively the same evolution of V_t, but the absolute values of V_t differ. Both the series show twinning with the onset of plastic deformation, twinning occurs at $\varepsilon = -0.4\%$ for series B, while the first twins for series A were observed at $\varepsilon = -0.5\%$. This difference is caused by higher CYS of series A. Then the formation of new twins could be observed in the large grains for both the series till a strain $\varepsilon \leq -1\%$ is reached. At higher strains only in some small grains a new formation of twins could be observed, while the existing twins begin to broaden. At $\varepsilon = -8\%$, the extension twinning is saturated for both the series and contraction twins can be activated [5].The differences in the absolute values of V_t of both the series are clearly attributed to the different grain sizes. Series A shows less V_t because of the finer grain structure. Nearby 40% of the initial microstructure of series A consist of very small DRX grains ($d < 3$ µm). According to the Hall–Petch relation the CRSS for twinning increases very strong with decreasing grain sizes, thus twinning occurs only, if these small DRX grains are in a favored orientation for twinning or local stress concentration supports twinning. That means that only the large grains, mainly the elongated grains and the few SRX grains, contribute to V_t, and the maximum value of $V_t \approx 62\%$ at $\varepsilon = -8\%$. For series B more SRX grains ($d = 20$–50 µm) were observed in the initial microstructure of the extrusions resulting in a stronger increase of V_t in the early stages of deformation and the maximum value of $V_t \approx 82\%$ at $\varepsilon = -8\%$. The evolution of V_t for series B is in good agreement with the data reported by [12] for samples with a average grain size of $d \approx 50$ µm, but the evolution of V_t of series A is different because of the smaller grain sizes.

Cyclic loading tests

This chapter gives an overview about the microstructures under cyclic loading conditions. First, the influence of the applied strain amplitude $5\% \geq \varepsilon_A \geq 1\%$ on the amount of twins and their characteristics will be analyzed for the samples of series A. Afterward the microstructural changes and formation of twins at very high numbers of cycles $N = N_f$ around the crack opening and under the fracture surface will be presented for series B.

Influence of the applied strain amplitude ε_A

Strain amplitude $\varepsilon_A = 5\%$ In order to analyze the progression of twinning during cyclic loading at $\varepsilon_A = 5\%$, the fatigue tests were stopped at characteristic numbers of cycles N either in the maximum of tensile or compressive strains. Figures 6, 7, and 8 show the cross-sections (perpendicular to the loading direction) of the tested specimens after $N = 1$, $N = 5$, and $N = 10$ cycles.

The twinned structure, generated during the first compressive half-cycle (Fig. 6a), is characterized by coarse and chunky twins (white). The total volume fraction of twins is about $V_t = 40\%$ and is in good agreement with the results of the compression tests performed for series A. Twin bands were observed in large grains only and show a width of 2–15 µm. The fine-grained DRX matrix ($d < 3$ µm) does not exhibit any twins due to the higher activation energy for twinning. However, all extension twins degenerate during the tensile half-cycle, because the tensile

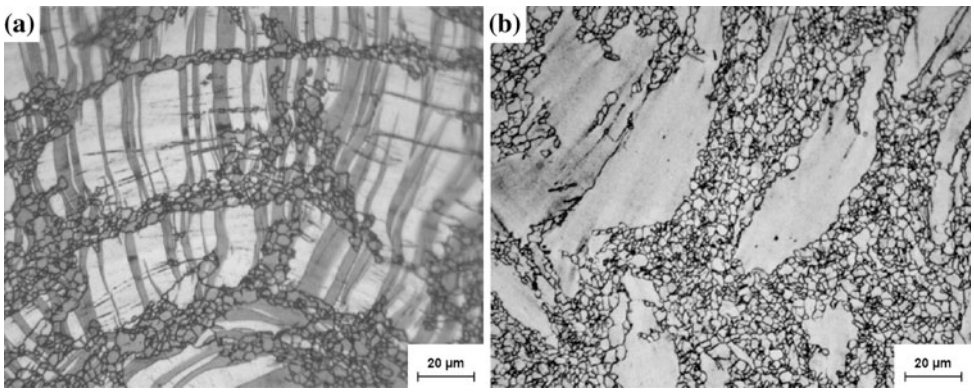

Fig. 6 Microstructural development (cross-sections) during cyclic loading at $\varepsilon_A = 5\%$: **a** $N = 1$, compressive maximum $\varepsilon_{A,min}$, **b** $N = 1$, tensile maximum $\varepsilon_{A,max}$

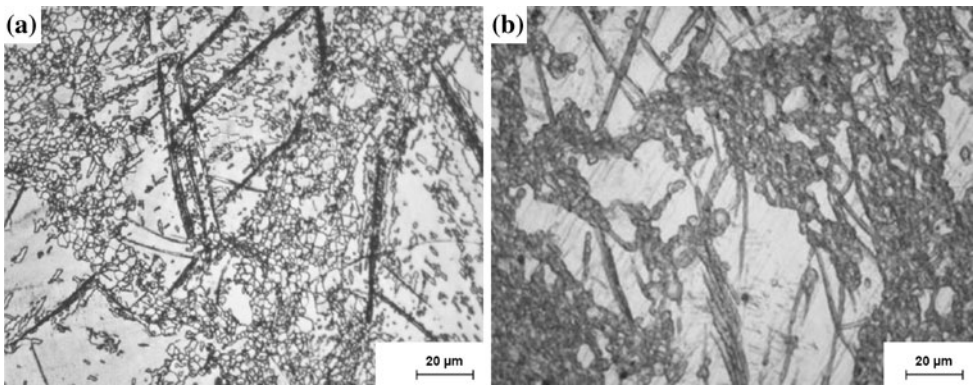

Fig. 7 Microstructural development (cross-sections) during cyclic loading at $\varepsilon_A = 5\%$: **a** $N = 5$, compressive maximum $\varepsilon_{A,min}$, **b** $N = 5$, tensile maximum $\varepsilon_{A,max}$

deformation after load reversal is mainly realized by detwinning [28–31]. When the detwinning mechanism is exhausted at about $\varepsilon \approx 0\%$ [30], slip systems have to be activated for further tensile deformation [30]. Consequently almost no extension twins were found in the tensile maximum of the first loading cycle (Fig. 6b). Also no $\{10\bar{1}1\}\langle 10\bar{1}2\rangle$ compressive twins, which usually occur during tensile deformation along the extrusion direction [8, 32], could be observed.

The plastic strain ε_{pl} during the first loading cycle for reaching the compressive maximum ($\varepsilon = -5\%$) was about $\varepsilon_{pl} = 4.5\%$, because we started at $\varepsilon = 0\%$. The subsequent tensile deformation up to the tensile maximum requires a plastic strain of about $\varepsilon_{pl} \approx 9\%$. With $N = 2$ and beyond a plastic strain about $\varepsilon_{pl} \approx 9\%$ is necessary to achieve the compressive maximum. This high plastic deformation results in a completely twinned microstructure, as it was observed in the compression tests for an applied strain of $\varepsilon \geq 8\%$. Consequently, no structures of the extension twinning system were observed in the compressive maximum at $N = 5$ (Fig. 7a).

The small and regularly formed twin structures observed in Fig. 7a are caused by the activation of $\{10\bar{1}1\}\langle 10\bar{1}2\rangle$ contraction twinning system, which was already observed in the compression tests at strains $\varepsilon > 8\%$ (Figs. 3f, 4f). At $N = 5$ in the tensile maximum the extension twins were completely detwinned, but the contraction twins are not detwinned and can still be observed in the large grains (Fig. 7b). With ongoing cyclic deformation up to $N = 10$ the amount of contraction twins increases and some of this twin structures show cleavages or even cracks due to the ongoing cyclic hardening. This development is shown in Fig. 8 for the compressive maximum and can be related to the cyclic hardening at $\varepsilon_A = 5\%$, which was also observed in [21].

For approving the findings obtained by optical microscopy, EBSD measurements were performed for $N = 1$ and $N = 5$ (Fig. 9). The poor quality of the orientation mapping could be explained by the very fine grain sizes of the DRX grains and thus a high fraction of grain boundaries. Additionally, a high defect density was generated during cyclic deformation, which also reduces the signal to noise ratio for the Kikuchi patterns and the indexing rate is decreased.

But the obtained orientation mappings are sufficient to prove the typical $\{10\bar{1}2\}\langle 10\bar{1}1\rangle$ extension twins (red) in the compressive maximum at $N = 1$ and the completely detwinned microstructure (blue again) in the tensile maximum at $N = 1$. At $N = 5$ a completely twinned microstructure (red) was detected for the compressive maximum, which completely detwins in the subsequent tensile maximum at $N = 5$. No $\{10\bar{1}1\}\langle 10\bar{1}2\rangle$ compressive twins could be indexed, because the quality of the patterns is too low.

Strain amplitude $\varepsilon_A = 3\%$ Figure 10 shows the development of extension twins in the compressive maximum

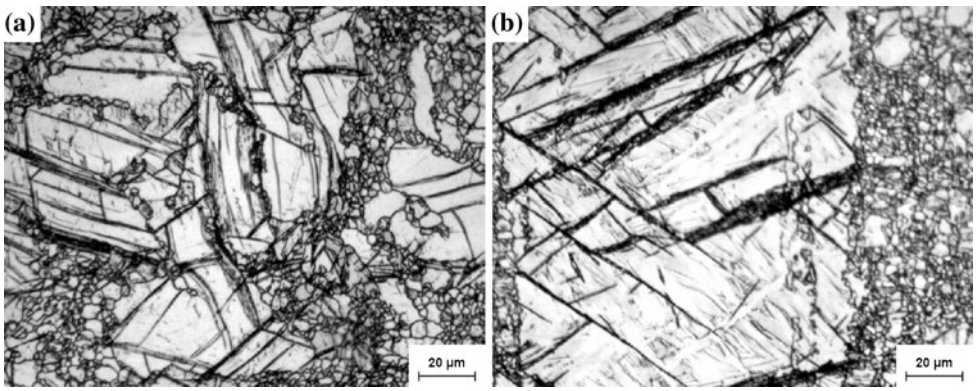

Fig. 8 Microstructural development during cyclic loading $\varepsilon_A = 5\%$ at $N = 10$ in the compressive maximum $\varepsilon_{A,min}$: **a** cross-section and **b** longitudinal section

during cyclic loading at applied strain amplitudes $\varepsilon_A = 3\%$. At $N = 10$ (Fig. 10a) twinning was observed in grains with diameter $d \geq 7$ µm. The twins are slightly curved and arranged almost parallel within one single grain. The width of the twins is about 1–4 µm and the total volume fraction is about $V_t \approx 41\%$. A slight increase in the volume fraction $V_t \approx 44\%$ was observed at a higher number of cycles $N = 57$ (Fig. 10b), short before failure.

But the major difference between the microstructures for $N = 10$ (Fig. 10a) and $N = 57$ (Fig. 10b) is the shape of the twins. With increasing N the twins show a reduced width, but there are some more twins and the distance between them is smaller. Furthermore, the twin bands appear more curved short before failure than it was observed at the beginning. The twin boundaries are more deformed and the parallel arrangement inside one single grain is no more existent. Twin structures, resulting from the activation of the $\{10\bar{1}1\}\langle 10\bar{1}2\rangle$ contraction twinning system, could not be found for a strain amplitude $\varepsilon_A \leq 3\%$,

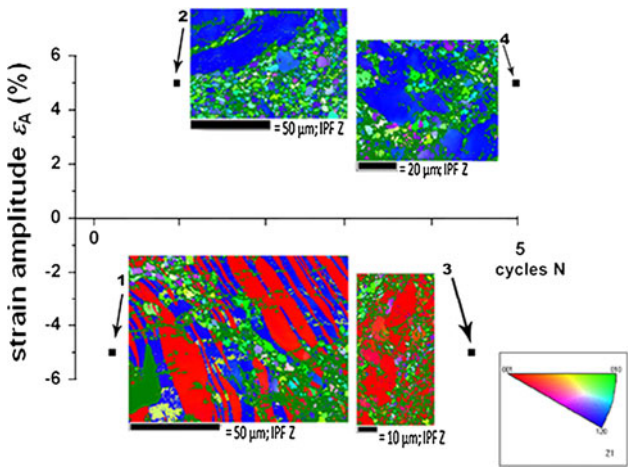

Fig. 9 EBSD images for an applied strain amplitude $\varepsilon_A = 5\%$: (*1*) $N = 1$, $\varepsilon_{A,min} = -5\%$, (*2*) $N = 1$, $\varepsilon_{A,max} = 5\%$, (*3*) $N = 5$, $\varepsilon_{A,min} = -5\%$, (*4*) $N = 5$, $\varepsilon_{A,max} = 5\%$

because the total plastic strain ε_{pl} between tensile and compressive maximum is only about $\varepsilon_{pl} \approx 5\%$.

Figure 11 shows the EBSD image measured on the cross-section of the sample loaded with $\varepsilon_A = 3\%$ and stopped in the compressive maximum at $N = 10$. The misorientation profile was measured within one single grain with the starting point as the reference. The misorientation angle between twins and "parent" grains is 86° ± 3° and proves the $\{10\bar{1}2\}\langle 10\bar{1}1\rangle$ extension twinning system.

Strain amplitude $\varepsilon_A = 1\%$ At low strain amplitudes $\varepsilon_A = 1\%$, the volume fraction ($V_t \approx 12\%$) and the width ($\sim$1–2 µm) of the extension twins in the compressive maximum at $N = 200$ (Fig. 12a) is lowered when compared to the samples described above, as a consequence of the lower plastic deformation.

The twins shown in Fig. 12 still exhibit a curvature, but are regularly arranged inside one grain. In contrast to the results for $\varepsilon_A = 5\%$, some residual extension twins in the tensile maximum (Fig. 12b, arrows) were observed, which were not completely detwinned. The exhaustion of the detwinning mechanism and the increase of residual twins were also reported by [29–31] for in situ diffraction studies of magnesium alloys during cyclic loading. The detwinning mechanism is hindered due to the higher defect density with increasing N [30, 31].

Strain amplitude $\varepsilon_A < 0.7\%$ If the strain amplitude ε_A is set only slightly above the elastic deformation limit ($\varepsilon_A = 0.5\%$ or $\varepsilon_A = 0.625\%$), characteristic accumulations of twins were observed at $N \approx N_f$ for the tested samples of series B (Fig. 13). Twin clusters were also found in the compression tests at the beginning of plastic deformation, but the accumulation of the twin structures after cyclic loading is more pronounced. These accumulations of twins were generated at Al–Mn particles or at stress concentrations as explained for the compression tests.

If the strain amplitude ε_A is lowered below the yield stress, no twins were formed in the bulk of the material

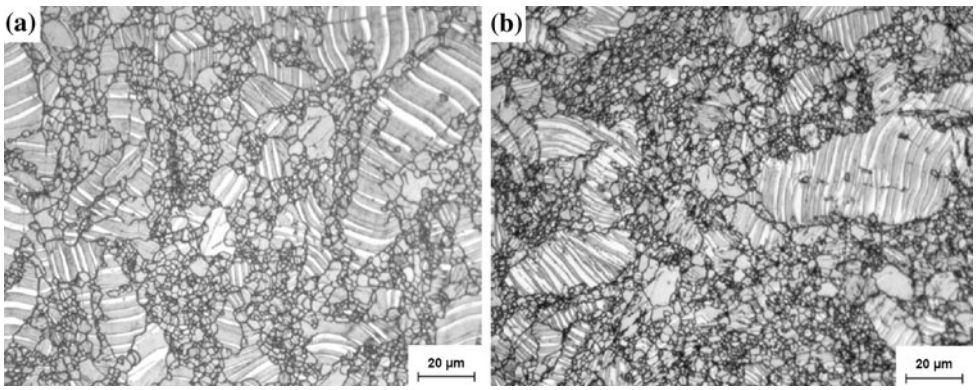

Fig. 10 Twinned microstructure (cross-sections) in the compressive maximum for $\varepsilon_A = 3\%$ at different numbers of cycles N: **a** $N = 10$ and **b** $N = 57$

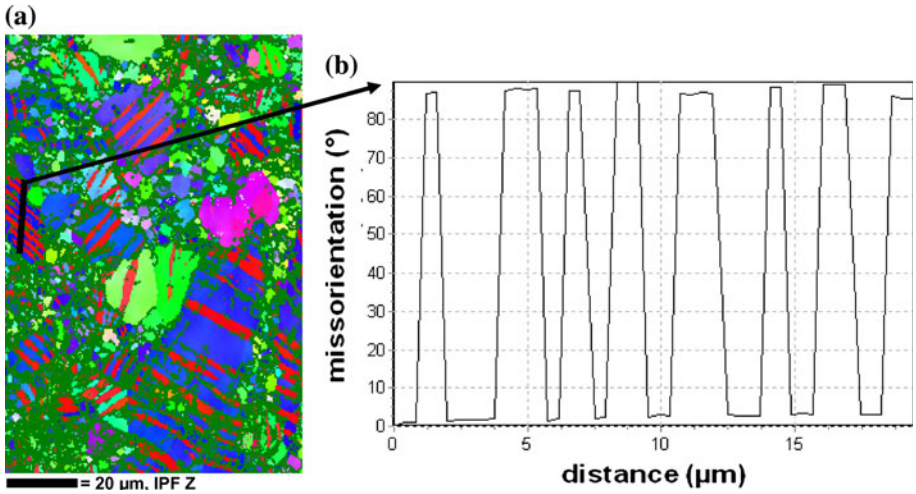

Fig. 11 **a** Orientation map (cross-section) for samples loaded with $\varepsilon_A = 3\%$ and stopped in the compressive maximum at $N = 10$; **b** misorientation profile (*black line*)

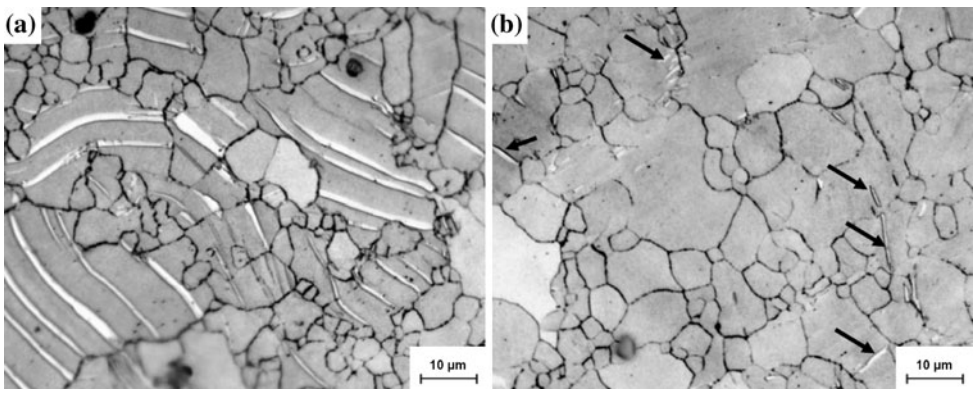

Fig. 12 Twinned microstructure (cross-sections) at $\varepsilon_A = 1\%$, stopped at $N = 200$: **a** compressive maximum and **b** tensile maximum

during cycle fatigue testing. At $\varepsilon_A < 0.4\%$, rupture occurs almost without the appearance of any twinning in the bulk material. Only some twins nearby the fracture surface were observed, which is discussed in the following.

Twin development near the fracture surface

The twinning behavior near the fracture surface differs significantly from the twinning behavior in the bulk material far away from the crack opening. Figure 14 shows the region around a crack tip for a sample (series B), which was loaded with $\varepsilon_A = 0.35\%$ and stopped in the tensile maximum at $N \approx 10^5$. The resulting microstructure after cyclic loading and crack propagation is differing at different positions of the surrounding of the crack tip, which results in varying fracture surface morphologies and different subsurface microstructures [24]. The region around the opened crack exhibits a high concentration of twins, while

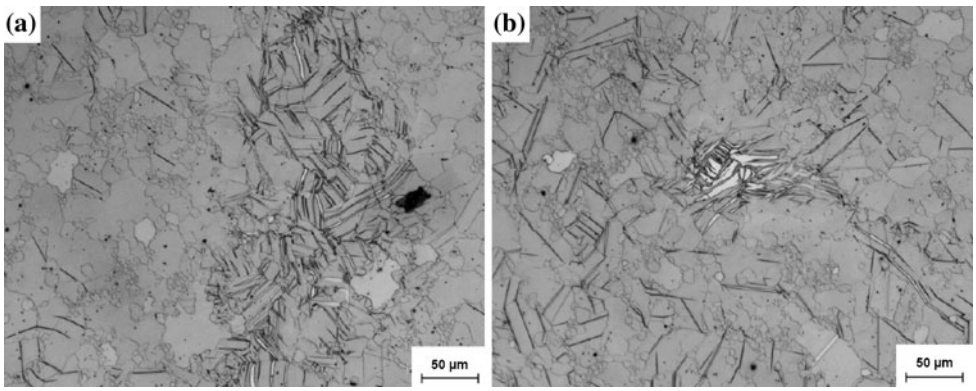

Fig. 13 Micrographs (cross-sections) showing accumulations of twins at low strain amplitudes stopped in the compressive maximum at $N \approx N_f$: **a** $\varepsilon_A = 0.5\%$ and **b** $\varepsilon_A = 0.625\%$

with increasing distance from the crack tip (perpendicular to the loading direction) no twins could be observed. The twin concentration is also lowered with increasing distance to the crack surface in loading direction.

Figure 15 relates the observed microstructure to the zone of the fracture surface for a sample (series A), which was loaded with $\varepsilon_A = 1\%$ until failure occurs in the tensile maximum at $N_f \approx 450$. Close to the crack opening surface the number of twins as well as the width is comparatively high (Fig. 14a). Near the crack propagation tip the amount of twinning decreases (Fig. 14b). Consequently, the twin bands get narrower. The overload rupture surface only exhibits some residual twins (Fig. 14c). The observed progress might be explained by the stress distribution of the specimen. During the compressive half-cycle twins are generated. Most of them detwin during the tensile half-cycle. If a crack is created, no tensile stresses can affect the microstructure nearby the crack opening. Consequently the twins cannot detwin in this zone. Although tensile stresses cannot operate in this area, compressive stresses can generate additional twins, if the crack is closed during the subsequent compressive half-cycle. During the overload rupture the tensile load detwins most of the twins in this region, but some residual twins are still visible.

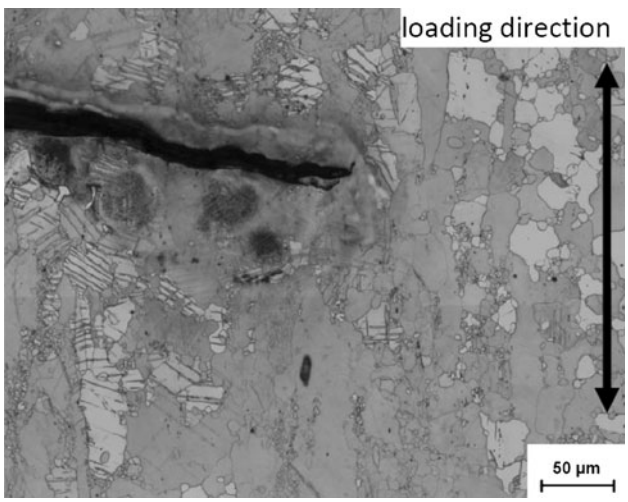

Fig. 14 Microstructure (longitudinal section) around a crack, series B at $\varepsilon_A = 0.35\%$, stopped in the tensile maximum at $N \approx 10^5$

Summary and conclusions

Quasi-static compression tests and fatigue tests have shown that the major part of the compressive plastic deformation is supported by the activation of the $\{10\bar{1}2\}\langle 10\bar{1}1\rangle$ extension twinning system. After saturation of the extension twinning system most of the grains are oriented with their *c*-axis parallel to the loading direction. Therefore, the $\{10\bar{1}1\}\langle 10\bar{1}2\rangle$ contraction twinning system can be activated, which is observed by microscopical analysis in form of straight and narrow twin bands.

The compression tests showed a significant influence of the initial grain size on the volume fraction V_t of the $\{10\bar{1}2\}\langle 10\bar{1}1\rangle$ extension twins. Both the series show primary twinning with the onset of plastic deformation, an exhaustion or saturation of the $\{10\bar{1}2\}\langle 10\bar{1}1\rangle$ twinning system at $\varepsilon = -8\%$ and the formation of $\{10\bar{1}1\}\langle 10\bar{1}2\rangle$ contraction twins at higher compressive strains $\varepsilon \geq -10\%$ (Figs. 3f, 4f).

But there are grain-size-dependent differences. In the case of series A, twinning starts at $\varepsilon = -0.5\%$, while in the case of series B with its lower CYS twinning sets in at $\varepsilon = -0.4\%$. The microstructure of the samples of series A exhibits very small ($d < 3$ µm) and very large grain sizes ($d > 20$ µm). Extension twins arise in the very large grains first. At $\varepsilon \approx -8\%$, the maximum amount of twins is obtained. It has to be noticed that twins are not observed in the very small grains ($d < 3$ µm), because the CRSS for twinning is still too high for these grains. Evidently plastic deformation in this regime is delivered by slip systems and a small amount of $\{10\bar{1}1\}\langle 10\bar{1}2\rangle$ contraction twins.

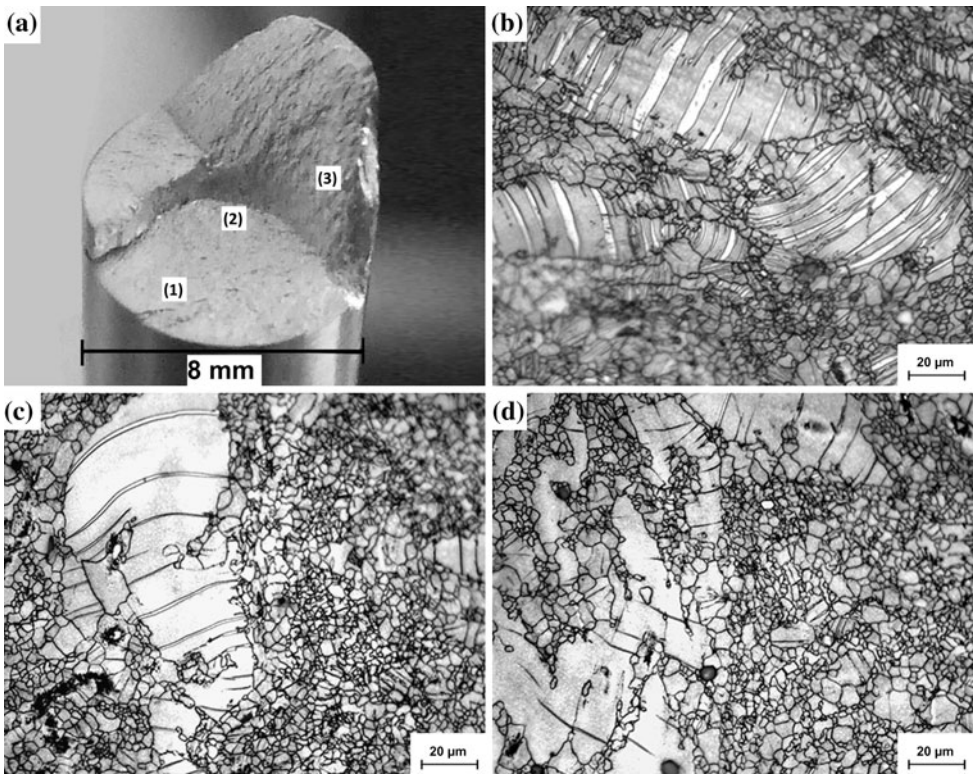

Fig. 15 Series A loaded with $\varepsilon_A = 1\%$ until failure: **a** fracture surface, **b** microstructure of position 1, **c** microstructure of position 2, and **d** microstructure of position 3

The initial microstructure of the samples of series B shows larger grains, which are more homogeneously distributed resulting in a more homogeneous distribution of extension twins after compressive deformation. The quantitative analysis of the volume fraction of twins V_t (Fig. 5) confirms the increase in twins for both the series with increasing compressive strains ε, but the quantitative values differ significantly. Series A shows a slower increase in V_t and a lower maximum at $\varepsilon = -8\%$ when compared to series B. The differences in the twinning characteristics and the V_t can be attributed to the grain-size-dependent CRSS for the activation of twins [4, 33].

Summarizing the most prominent results of the tests under cyclic loading conditions typical microstructures observed in the compressive maxima after cyclic loading for $\varepsilon_A \geq 1\%$ are displayed in Fig. 16.

Figure 16 shows that the volume fraction V_t and the especially the width of $\{10\bar{1}2\}\langle 10\bar{1}1\rangle$ extension twins increases with increasing ε_A corresponding to the increasing plastic strain amplitude $\varepsilon_{A,pl}$. The samples presented in Fig. 16 were stopped long before failure N_f, thus the twin boundaries are only slightly deformed and curved. At $N \approx N_f$ an increase in the irregularity of twin formation was shown for $\varepsilon_A = 3\%$ (Fig. 10b). For $\varepsilon_A = 5\%$, higher N result in a completely twinned microstructure in the compressive maximum and a completely detwinned microstructure in the tensile maximum, but contraction twins (Figs. 7, 8) could be observed in both maxima.

During the tensile half-cycle the extension twins completely detwin at very high $\varepsilon_A \geq 3\%$, because only small N_f can be realized. However, if cyclic testing proceeds to higher N at $\varepsilon_A \leq 1\%$, some residual extension twins are still observed in the tensile maximum. This amount of these residual extension twins increases with increasing number of cycles N during fatigue testing. This finding is approved by in situ diffraction studies during cyclic loading [28–31].

At strain amplitudes $\varepsilon_A < 0.7\%$, the quantity and the number of twin bands decreases strongly, because of the low plastic deformation. Fatigue tests carried out at strain amplitudes ε_A slightly above the yield point exhibit areas of twin accumulation, which are more pronounced when compared to the quasi-static compression tests. These accumulations occur mainly at Al–Mn particles and at regions of stress concentrations. The more pronounced twin accumulation is also caused by the ongoing cyclic hardening behavior and by the presence of residual extension twins in the tensile maximum.

When the cracks are initiated and crack propagation proceeds, only compressive stresses are present nearby the crack propagation surface. As a consequence the twins do not detwin during the tensile half cycle. In the subsurface area of the overload rupture only some residual twins are present, which are not detwinned during the tensile rupture.

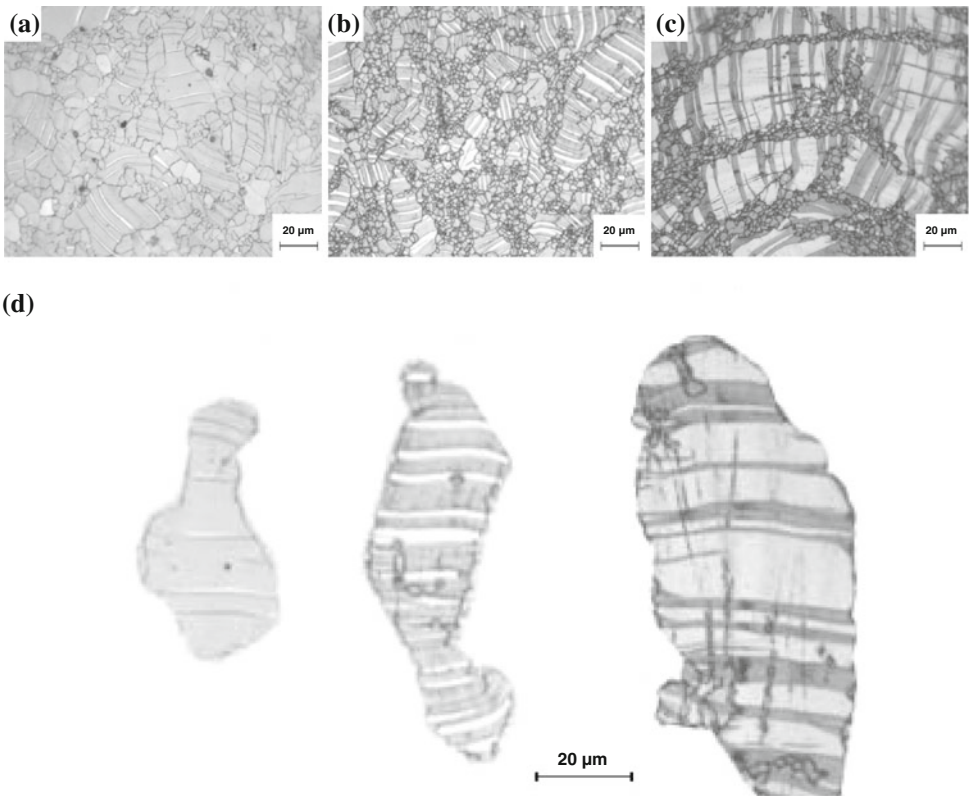

Fig. 16 Twinned microstructure (cross-sections) observed in the compressive maximum for different strain amplitudes ε_A and number of cycles N: **a** $\varepsilon_A = 1\%$, $N = 200$, **b** $\varepsilon_A = 3\%$, $N = 10$, **c** $\varepsilon_A = 5\%$, $N = 1$, and **d** comparison of selected grains

However, most of the twins detwin due to the intense tensile load.

Acknowledgements The authors are grateful for the financial support from the Deutsche Forschungsgemeinschaft (DFG) under the contract number Re 688/59-1-2. Special thanks goes to Elif Altunay (Metallic Materials, TU Berlin) for helping with the metallographic preparation analyses and to Jörg Nissen (ZELMI, TU Berlin) for the assistance during the EBSD measurements.

References

1. Yoo MH (1981) Metall Trans A 12:409
2. Yoo MH, Morris JR, Ho KM, Agnew SR (2002) Metall Mater Trans A 33:813
3. Agnew SR, Tomé CN, Brown DW, Holden TM, Vogel SC (2003) Scripta Mater 48:1003
4. Barnett MR, Keshavarz Z, Beer AG, Atwell D (2004) Acta Mater 52:5093
5. Brown DW, Agnew SR, Bourke MAM, Holden TM, Vogel SC, Tomé CN (2005) Mater Sci Eng A 399:1
6. Yi SB, Davies CHJ, Brokmeier H-G, Bolmaro RE, Kainer KU, Homeyer J (2006) Acta Mater 54:549
7. Barnett MR (2007) Mater Sci Eng A 464:1
8. Barnett MR (2007) Mater Sci Eng A 464:8
9. Lou XY, Li M, Boger RK, Agnew SR, Wagoner RH (2007) Int J Plast 23:44
10. Huppmann M, Reimers W (2010) Microstructure and mechanical properties of differently extruded AZ31 magnesium alloy. Int J Mater Res (accepted)
11. Bohlen J, Yi SB, Swiostek J, Letzig D, Brokmeier HG, Kainer KU (2005) Scripta Mater 53:259
12. Jiang L, Jonas JJ, Mishra RK, Luo AA, Sachdev AK, Godet S (2007) Acta Mater 55:3899
13. Bohlen J, Dobron P, Swiostek J, Letzig D, Chemlik F, Lukac P, Kainer KU (2007) Mater Sci Eng A 462:302
14. Jiang J, Godfrey A, Liu W, Liu Q (2008) Mater Sci Eng A 483–484:576
15. Noster U, Scholtes B (2003) Z Metallkd 94:559
16. Noster U (2003) Universität Kassel, PhD-thesis
17. Hasegawa S, Tsuchida Y, Yano H, Matsui M (2007) Int J Fatigue 29:1839
18. Lin XZ, Chen DL (2008) Mater Sci Eng A 496:106
19. Begum S, Chen DL, Xu S, Luo AA (2009) Int J Fatigue 31:726
20. Matsuzuki M, Horibe S (2009) Mater Sci Eng A 504:169
21. Huppmann M, Brömmelhoff K, Reimers W (2009) In: Kainer KU (ed) Proceedings of the 8th international conference on magnesium alloys and technology, vol 740. Wiley-VCH, Weinheim
22. Huppmann M, Lentz M, Brömmelhoff K, Reimers W (2010) Mater Sci Eng A 527:5514
23. Yang F, Yin SM, Li SX, Zhang ZF (2008) Mater Sci Eng A 491:131
24. Yin SM, Yang F, Yang XM, Wu SD, Li SX, Li GY (2008) Mater Sci Eng A 494:397
25. Yin SM, Yang HJ, Li SX, Wu SD, Yang F (2008) Scripta Mater 58:751
26. Yang HJ, Yin SM, Huang CX, Zhang ZF, Wu SD, Li SX, Liu YD (2008) Adv Eng Mater 10:955
27. Rasband W ImageJ 1.42q. http://rsb.info.nih.gov/ij (23.12.2009), for Java 1.6.0_10(32bit)
28. Wu L, Jain A, Brown DW, Stoica GM, Agnew SR, Clausen B, Fielden DE, Liaw PK (2008) Acta Mater 56:688
29. Brown DW, Jain A, Agnew SR, Clausen B (2007) Mater Sci Forum 539–543:3407

30. Huppmann M, Stark S, Reimers W (2010) Int J Mater Res. doi: 10.3139/146.110378
31. Huppmann M, Stark S, Reimers W (2010) Mater Sci Forum Vols 638–642:2411
32. Yi SB, Brokmeier H-G, Bolmaro RE, Kainer KU, Lippmann T (2004) Scripta Mater 51:455
33. Meyers MA, Vöhringer V, Lubarda A (2001) Acta Mater 49:4025